Available online at www.sciencedirect.com
SCIENCE DIRECT®
Optics Communications 242 (2004) 517–524
OPTICS COMMUNICATIONS
www.elsevier.com/locate/optcom

High-efficiency coupling between external and photonic crystal waveguides by longitudinally shifting waveguide junctions

Chun-Wen Chang [a], Szu-Cheng Cheng [b], Wen-Feng Hsieh [a,*]

[a] Institute of Electro-Optical Engineering, National Chiao Tung University, Hsinchu, Taiwan, ROC
[b] Department of Physics, Chinese Culture University, Yang Ming Shan, Taipei, Taiwan, ROC

Received 31 March 2004; received in revised form 1 August 2004; accepted 6 September 2004

Abstract

Longitudinally shifting waveguide junctions can achieve high efficiency light coupling from external silica waveguides into photonic crystal waveguides (PCWs) without requiring taper PCW structures in the waveguide junctions. Due to the periodic field distribution of PCWs along the propagation direction, maximum and minimum coupling efficiency occur when waveguide junctions are located near the peak and valley of the longitudinal mode profile, and coupling efficiency depends on both the localization of mode fields in PCWs and the group velocities of eigenmodes. Coupling efficiency of 86% between silicon/silica PCWs and external silica waveguides can be achieved without the need for special design in the junction region for the reduced-rod PCW. Due to large Bragg reflection, coupling of the band edge modes at the flat dispersion regions that possess small group velocities is inefficient.
© 2004 Elsevier B.V. All rights reserved.

Keywords: Photonic crystal waveguide; Coupling efficiency; Optical waveguide; Periodic structures; Bragg reflection; Integrated optics

1. Introduction

Photonic crystal waveguides (PCWs), constructed by introducing line defects in photonic bandgap (PBG) structures, provide a potential approach for achieving ultra-compact photonic integrated circuits (PICs). Because of their superior ability to control and confine light propagation within the PBG in photonic crystals (PhCs), PCWs can confine the propagation of light effectively even with a sharp bend [1]. In this manner, various integrated photonic devices have been demonstrated in use of PCWs [2–4]. However, a key obstacle limiting the applications of PCWs in PICs is to develop a method of efficiently coupling light between PCWs and external lightwave circuits.

To achieve high coupling efficiency between external waveguides and PCWs, various analyses

* Corresponding author. Tel.: +886 3 5712121/56316; fax: +886 3 5716631.
E-mail address: wfhsieh@mail.nctu.edu.tw (W.-F. Hsieh).

0030-4018/$ - see front matter © 2004 Elsevier B.V. All rights reserved.
doi:10.1016/j.optcom.2004.09.016

have been performed to improve the transverse mode-profile matching [5–12] at the junction of the external waveguide and the PCW. Among these structures, the external waveguide tapers and the PCW tapers with the localized defects have been shown capable to convert the transverse mode profiles of the external waveguides to match those of the PCWs [7]. These methods merely consider the transverse mode matching and ignore the mode-profile variation in the longitudinal direction. However, due to the periodicity of a PCW structure, the modal field in a PCW is a Bloch state [10]. That is, the transverse mode profiles of the PCWs vary periodically along the propagation (or longitudinal) direction. This periodic variation characteristic of the modal field implies that the coupling efficiency of an external dielectric waveguide with a PCW should depend on the position of junction between these two waveguides. To demonstrate the need to consider the mode matching longitudinally, in this investigation we analyze the coupling efficiency as a function of the longitudinal position of the junction and find the optimum coupling position.

The PhC analyzed in this study is a rod structure PhC, where the PhC is formed by high refractive index rods surrounded by a lower index medium. The single-line-defect rod structure PCW with single guided mode inside the PBG significantly improves the performance of PIC devices [13]. As seen in Fig. 1, we analyzed the coupling efficiency of two general rod structure PCWs, i.e., the removed-rod and the reduced-rod PCWs, both of which are butt coupled to the external waveguides. This study analyzed the band structures and the stationary mode profiles of the PCWs using the plane-wave expansion method and calculated the transmittances as a function of the longitudinal position of the waveguide junction by the two-dimensional (2-D) finite-difference time-domain (FDTD) method. The butt coupling of the removed-rod PCWs is analyzed and the coupling efficiency is shown to be less than 30% without any special design at the waveguide junction [7]. However, by properly shifting the junction position along the longitudinal direction, the coupling efficiency of the removed-rod PCWs can be increased to up to 70% readily. The same technique can be applied to the reduced-rod waveguide and the coupling efficiency of up to 86% can be achieved. Additionally, the transmission spectra of the reduced-rod PCWs are also analyzed to

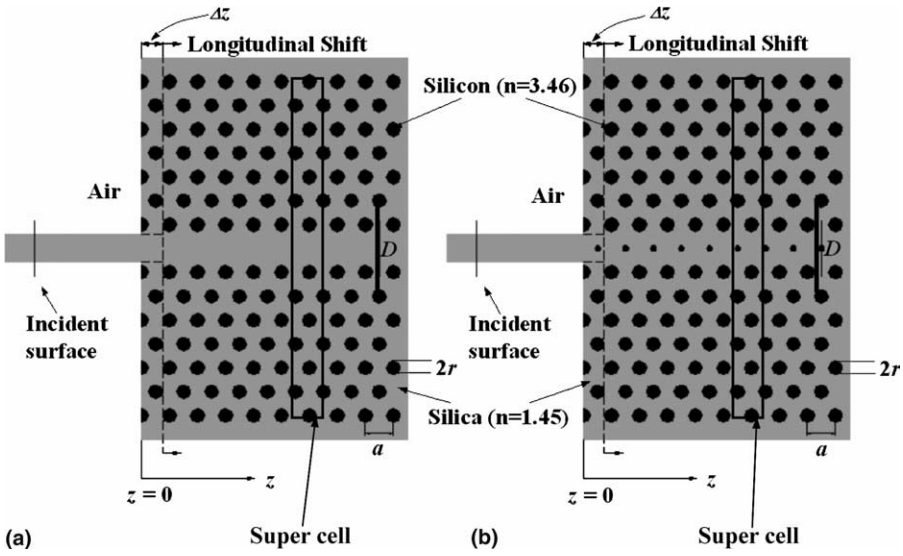

Fig. 1. Schematic of the structures analyzed for coupling from an external waveguide to the PCWs including: (a) the removed-row PCW and (b) the reduced-row PCW. The incident waves are excited on the incident surface and the transmission flux is integrated along the plane D while the waveguide junctions successively move from $z = 0$ toward the right.

show that the proposed method is very intuitive and suitable for designing high-efficiency and wide-bandwidth coupling structures.

2. Analysis method

The PhC structure analyzed in this work is composed of a 2-D triangular lattice of silicon rods surrounded by silica. This rod structure PhC has been investigated in previous studies [2,7,13] and demonstrated experimentally in a silicon-based PIC [14]. The radii of the silicon rods of this photonic crystal are assumed to be $r = 0.25a$, where a denotes the lattice constant. The refractive indices of the silicon rods and the ambient silica are taken to be 3.46 and 1.45, respectively, at the wavelength $\lambda = 1.55$ μm. With these parameters, this triangular lattice exhibits a bandgap of transverse magnetic (TM) modes in the normalized frequency range $f = 0.2359$–$0.3258c/a$, where c represents the speed of light in vacuum. From Fig. 1, the PCWs investigated in this study were created by removing a row of rods [type A, Fig. 1(a)] and reducing the radii of the whole row of rods to $r_d = 0.1a$ [type B, Fig. 1(b)] along the Γ–K direction of the PhC. Fig. 2 displays the band structures of the PCWs obtained using a 2-D plane-wave expansion method [15], which computes the Bloch wave vector k using the super cell enclosed in the boxes in Fig. 1. From Fig. 2, the gray areas denote regions of the extended modes of the perfect PhC. Moreover, the solid and dashed lines within the bandgap represent the dispersion curves of the type-A (removed-rod) and type-B (reduced-rod) PCWs, respectively. Both types of waveguides have a single guided mode inside the PBG.

To investigate the longitudinal mode profiles of the PCWs, the stationary intensity distributions of the four modes A1, A2, B1, and B2, labeled on the dispersion curves in Fig. 2, were calculated by means of the plane-wave method and presented in Figs. 3(a)–(d), respectively. These modes include two type-A PCW modes: A1 for $f = 0.290$ c/a and A2 for $f = 0.314c/a$ located near the band center and band edge, respectively, and both these two modes are situated in the slope region of the dispersion curve. The B1 mode, corresponding to the type-B PCW mode for $f = 0.287c/a$ situated near the band center. Besides, to investigate the coupling issues of the modes with strong interaction between forward and backward fundamental Bloch modes, we also study the B2 mode ($f = 0.3c/a$), which is located near the flat region of the dispersion curves with very small group velocity. The modes A2, B1, and B2 are located below the light line of vacuum. Thus all of these modes are expected to be confined in PCW slabs.

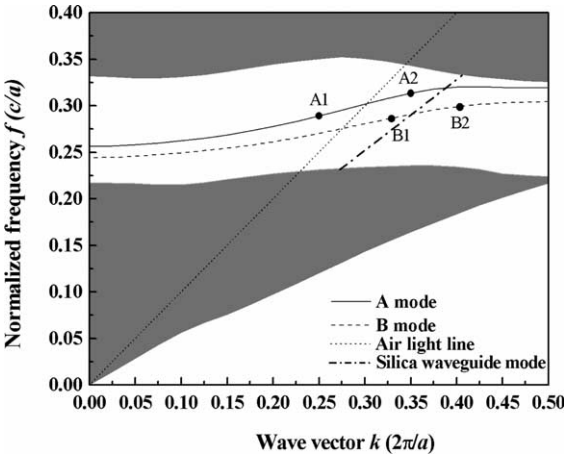

Fig. 2. Band structure of the type-A PCW (solid line) and type-B PCW (dash line). The A1, A2, B1, and B2 are four modes analyzed in this study. The gray areas represent the extended modes of the bulk PhC.

From Fig. 3, the electric energy distributions ($\epsilon|E|^2$) of these four modes vary not only laterally but also periodically along the longitudinal direction in the PCWs. Additionally, the periodic variations of the longitudinal modal fields have the same periods as the lattice of the original PhCs. The optical energy is localized around the original positions of the silicon rods. The localization of the modal fields depends both on the types of PCWs and on the frequencies of the waveguide modes. The modal field of the type-B PCW (reduced-rod PCW) is more localized than that of the type-A (removed-rod) PCW, and the near-band-edge mode (A2 mode) displays more significant field localization than the band center mode (A1 mode). Especially, the light field of the type-B PCW is confined as a standing wave within the

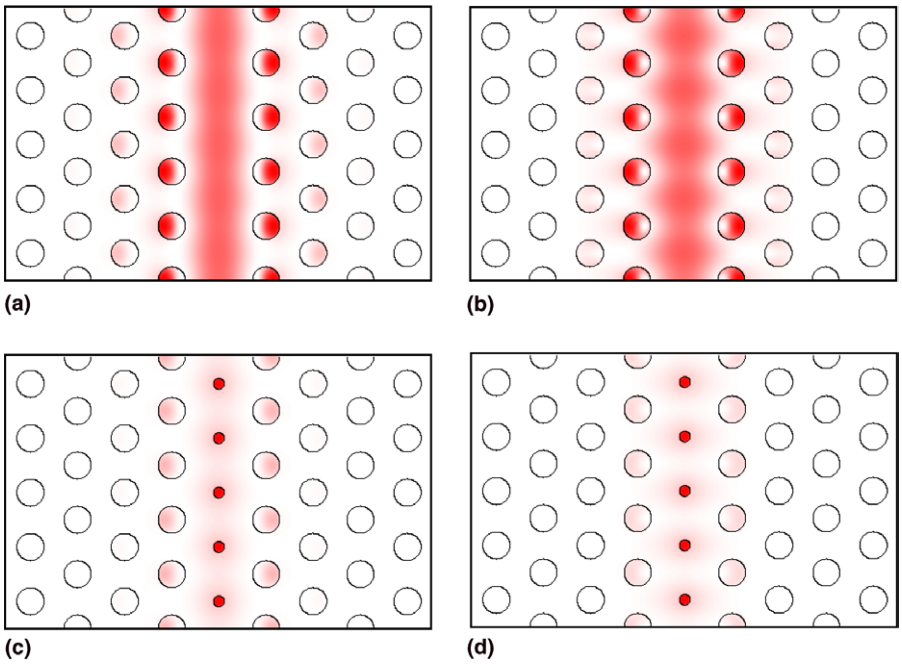

Fig. 3. Stationary intensity profiles of the (a) A1 mode, (b) A2 mode, (c) B1 mode and (d) B2 mode.

defect rods [see Fig. 3(c)], which covers less than one-tenth of wavelength.

If we ignore the coupling to the backward components of fundamental Bloch modes, the dependence of the coupling efficiency η on the longitudinal positions of waveguide junctions between PCWs and conventional waveguides can be conceptually explained by the following overlap integral:

$$\eta = \left[\int E_{ex}(x)E^{*}_{pc}(x)\,dx\right]^{2} \Big/ \int E_{ex}(x)E^{*}_{ex}(x)\,dx \times \int E_{pc}(x)E^{*}_{pc}(x)\,dx$$

[16], which is successfully employed to study coupling issues between z-invariant waveguides. Here E_{ex} and E_{pc} represent the mode fields of the external and the PhC waveguides, respectively, and x is the transverse coordinate. According to the above relation, since E_{pc} varies periodically along the longitudinal direction, the coupling efficiency should depend on the junction location, and will significantly improve as the waveguide junction approaches the field-localized point of the PCWs.

This study uses silica as the material of the feeding waveguide, which can more easily couple with optical fibers through a waveguide taper than other high-index materials. We feed optical power into the PCW through the air-clad silica waveguide, with the waveguide width $w_g = 1.0a$. The dispersion curve of the feeding waveguide is also shown in Fig. 2. In this case, the external waveguide is excited by the fundamental mode of $\lambda = 1.55$ μm from the incident plane in Fig. 1. The length L of the PCW is $10a$, and the PCW is surrounded by seven rows of rods on each side. The perfect match layer conditions are considered in the FDTD calculation to avoid the reflection of radiation waves in the boundaries of the calculation domain. To identify the optimum coupling point of the waveguide junction, as illustrated in Fig. 1, the transmittances from the external waveguides to the PCWs are calculated using the FDTD method by shifting the waveguide junction with a step of $\Delta z = 0.1a$. During moving the junction forward, the remainder of

the PhC cladding behind the junction (the PhC cladding in the Δz region) was removed and became air, which could be achieved by dry etching technology. A resolution of 40 grid points per lattice is employed to ensure accurate modeling of the $0.1a$ longitudinal shift. The transmittance T is calculated by integrating the Poynting vector over the integration plane D in Fig. 1 and then is normalized to the input power while the waveguide junctions successively move from $z = 0$ toward the right. Since the contribution of radiation fields in the PCW will affect the accuracy of the integrated transmission power, the longitudinal position of the integration plane D should be far enough to ensure that the stationary mode field has been reached. Therefore, we calculate the transmittance as a function of the longitudinal position of the plane D, and find that the calculated result converges to a constant as long as the integration plane D is farther than $z = 5.5a$. As can be seen in Fig. 1, the integration plane D is located at a distance of $z = 8.5a$, and is extended to the second row of rod in PhC claddings to ensure that it is wide enough to cover most of the PCW mode. Furthermore, for examining the coupling bandwidth, the transmission spectrum of the reduced-rod PCW, which has the highest coupling efficiency, is also analyzed.

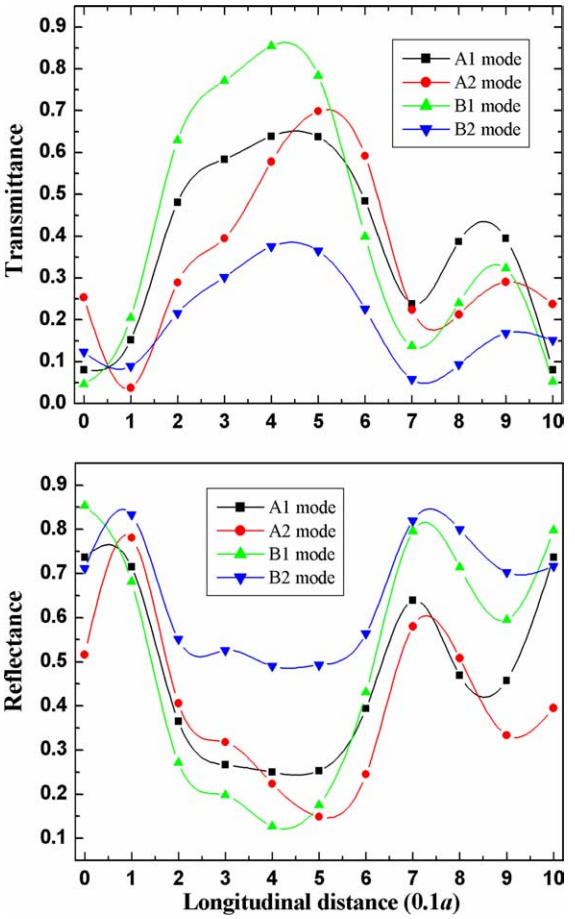

Fig. 4. Transmittances and reflectances of the A1, A2, B1, and B2 modes as a function of the longitudinal positions of the waveguide junction between external waveguides and PhC waveguides.

3. Results and discussion

Fig. 4 shows the transmittances (T) and the reflectances (R) as a function of the longitudinal position of waveguide junctions, which originates from the valley point of the PCW where the modal field intensity of the PCW is minimal. Since the radiation scattering losses from the modal mismatch is not collected by the detector, which collect the reflected guided waves only within the silica waveguides, the sum of the transmittance and the reflectance is not equal to unity. The transmittances of these four modes vary considerably as the waveguide junction shifts longitudinally, and all of them reach their maxima when the waveguide junctions are located near the maximal intensity of the modal fields of the PCWs. On the other hand, the transmittance is very low when the waveguide junction is near the valley position of the PCW. In addition to the positions of the waveguide junctions, the group velocities of eigenmodes and the PCW types also significantly affect coupling efficiency.

As can be seen in the B1–PCW mode with the stronger field localization than the type-A PCW mode and the highest coupling efficiency, the transmittance reaches up to 86% when the waveguide junction is near the maximum intensity position, and is below 5% when the waveguide junction is near the valley position. In the B2 mode, the mode field is even more localized than that of the

B1 PCW mode [Fig. 3(d)]. We would have expected that the transmittance of the B2 mode were higher than that of the B1 mode. However, in Fig. 4, we found that the B2 mode has much less transmittances (maximum efficiency < 40%) but very high reflectances. Besides, the modulation depths of both the transmittance and reflectance along the longitudinal position for the B2 mode are much less than those of the B1 mode. Notice that the summations of the transmittance and reflectance for both modes almost reach 90%. Most of the energy in the B2 mode is reflected with the maximum reflectance of 82% ($z = 0.1a$), and $R = 50\%$ even when the waveguide junction is near the maximum intensity position ($z = 0.4a$), where has the maximum transmittance $T = 39\%$. This may be partly because of the large group velocity mismatch between the feeding silica waveguide mode and the B2 mode which has a far smaller group velocity, and partly because of Bragg reflection when the operation frequency of the PCW mode such as B2 is close to the band edge where the PCW mode is resemble to the standing wave not just within the defect rods. On the other hand, since both the A1 and A2 modes locate in the slope region of the dispersion curve, the group velocities of these two modes are similar and the difference of the coupling efficiency between these two modes is unapparent. If we shift the A2 mode to the flat region of the dispersion curve (e.g., $k = 0.42\pi/a$, $f = 0.32c/a$), the reflectance at the optima junction position ($z = 0.6a$) grows up 40% due to the backward coupling from large Bragg reflection and group velocity mismatches. However, the summation of the R and T is only 67% at the optima junction position since this flat-dispersion mode strongly couples with leaky modes to cause serious radiation losses. From the FDTD simulation (not shown here) we can see that the field extends over the bulk PhC regions. Furthermore, the calculated transmittances as a function of the longitudinal position do show asymmetry however the E_{pc} is symmetric within the lattice period. Thus the classical approximate formula of the overlap integral, which considers only fundamental forward Bloch modes, is not suitable to predict the coupling of rod structure PCW modes with considerable backward components.

To obtain a further insight into the high-efficiency coupling of the type-B (reduced-rod) PCW, the electric fields of the input coupling between the external waveguide and the type-B PCW at the maximal and minimal transmittances were calculated using the FDTD method. Strong coupling (86%) clearly occurs [see Fig. 5(a)] when the waveguide junction is located near the center of the defect ($z = 0.4a$) where the light field is strongly localized. On the other hand, weak coupling (4.5%) occurs [see Fig. 5(b)] when the waveguide junction is situated at the point of minimum modal field intensity ($z = 0$). In this case, the incident optical field is mostly reflected at the waveguide junction owing to the significant modal

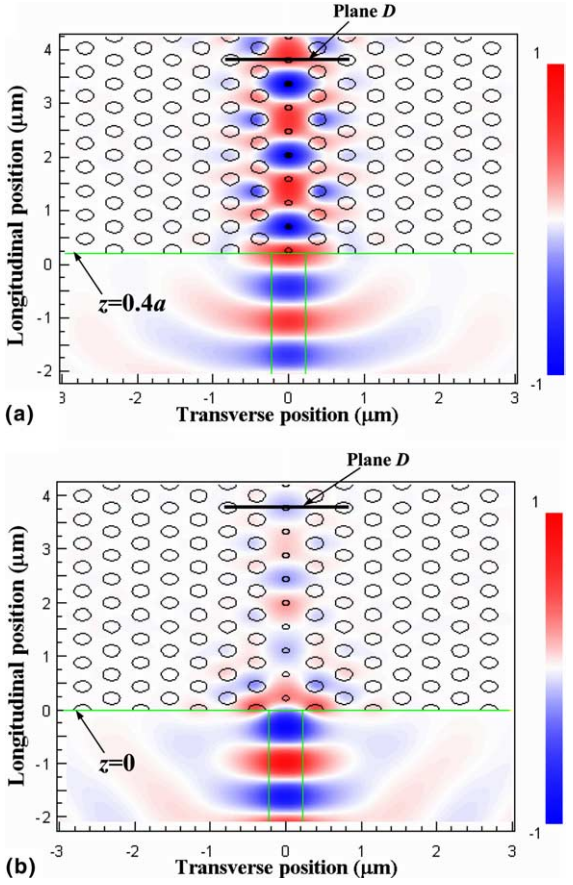

Fig. 5. Snapshots of the electric field distributions for: (a) maximum ($z = 0.4a$) and (b) minimum ($z = 0$) transmittance of the B1 mode.

mismatch. Besides, since the time-domain electric field distribution of a Bloch mode depends on both PhC periodicities and wave vectors, the field patterns shown in Fig. 5 also display the wave vector induced periodicity. To investigate the effect of wave vectors, we calculate the transmittance of the B1 mode ($k = 0.3212\pi/a$) as a function of the longitudinal position for two periods of the PhC and find that the difference between these two cycles is less than 1%. Therefore, the wave vector induced periodicity would not affect the physical explanation of the optimum junction location.

To examine the coupling bandwidth of the proposed scheme, we analyzed the transmission spectrum of the B1–PCW mode with the external waveguide at the maximum coupling efficiency. From Fig. 6, the transmittance exceeds 77% within the frequency range $f = 0.247$–$0.289c/a$ (corresponding to $\lambda = 1539$ to 1801 nm). On both extreme ends of the transmission spectrum, the coupling efficiency abruptly drops to almost zero. That is because of large Bragg reflection for the band edge modes as mentioned earlier. Consequently, coupling between external and PhC waveguides varies with the longitudinal position of the junction, and high efficiency and wide bandwidth coupling of the reduced-rod PCW can be achieved by locating the junction near the peak of the longitudinal mode profile.

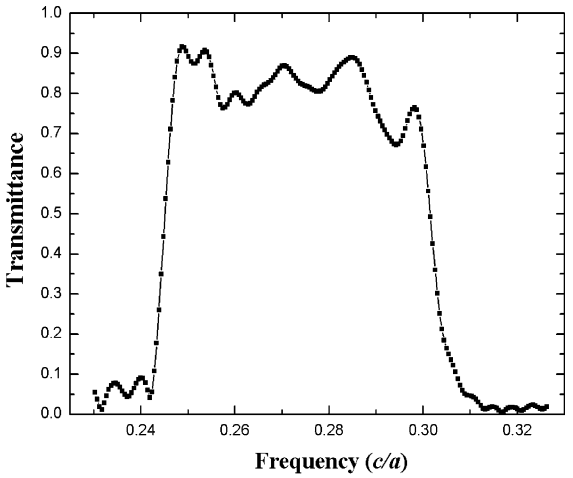

Fig. 6. Transmission spectrum for the B1–PCW mode with the external waveguide at the maximum coupling efficiency.

4. Conclusion

To summarize, this study presented a convenient method for high-efficiency coupling between external and PhC waveguides by shifting the waveguide junction longitudinally. The distribution of the PCW mode field was calculated using the plane-wave expansion approach, and was found to vary periodically along the PCW. The localization of the modal field in the PCW depends on both the waveguide structure and the eigenmode frequency. High-efficiency coupling can be achieved by conveniently shifting the waveguide junction near the peak position of the longitudinal mode profile. Additionally, the coupling efficiency depends on both the types of PCWs and the group velocity of Bloch modes. The B1 mode of the type-B (reduced-rod) waveguide located near the band center with a strongly localized field and a high group velocity has the best coupling with the silica waveguide. In practical PCW slabs, out-of-plane scattering losses in cladding layers due to modal mismatches should be significant [10,17], and the dispersion curves will be shifted for some frequency range because of the index confinement in the perpendicular direction in a real PCW slab [5]. Using 2-D calculations one might be able to identify the function of the coupling structure qualitatively in the PCW slabs before performing three-dimensional (3-D) exact electromagnetic analyses, which can be used to achieve more quantitative results. Therefore, the proposed concept can be combined with planar tapered waveguides [18] to achieve high efficiency and wide bandwidth coupling between external silica and silicon/silica PhC waveguides in PICs. Furthermore, since these flat dispersion PCW modes with small group velocities are very useful to design novel PIC devices, the efficient coupling of the band edge modes should be a challenging work that must be investigated.

Acknowledgment

This work is partially supported by the National Science Council and the Ministry of Economics Taiwan under Grants NSC-92-2112-M009-037 and 92C240.

References

[1] M. Tokushima, H. Kosaka, A. Tomita, H. Yamada, Appl. Phys. Lett. 76 (2000) 952–954.
[2] A. Martinez, F. Cuesta, J. Marti, IEEE Photon. Technol. Lett. 15 (2003) 694–696.
[3] K. Hosomi, T. Katsuyama, IEEE J. Quantum Electron. 38 (2002) 825–829.
[4] J. Zimmermann, M. Kamp, A. Forchel, R. Marz, Opt. Commun. 230 (2004) 387–392.
[5] N. Molla, G.-L. Bona, J. Appl. Phys. 93 (2003) 4986–4991.
[6] P. Pottier, I. Ntakis, R.M. De La Rue, Opt. Commun. 223 (2003) 339–347.
[7] P. Sanchis, J. Marti, A. Garcia, A. Martinez, J. Blasco, Electron. Lett. 38 (2002) 961–962.
[8] D.W. Prather, J. Murakowski, S. Shi, S. Venkataraman, A. Sharkawy, C. Chen, D. Pustai, Opt. Lett. 27 (2002) 1601–1603.
[9] E. Miyai, M. Okano, M. Mochizuki, S. Noda, Appl. Phys. Lett. 81 (2002) 3729–3731.
[10] Ph. Lalanne, A. Talneau, Opt. Express 10 (2002) 354–359.
[11] T.D. Happ, M. Kamp, A. Forchel, Opt. Lett. 26 (2001) 1102–1104.
[12] A. Mekis, J.D. Joannopoulos, J. Lightwave Technol. 19 (2001) 861–865.
[13] A. Martinez, J. Garcia, G. Sanchez, J. Marti, J. Opt. Soc. Am. A 20 (2003) 2131–2136.
[14] M. Tokushima, H. Yamada, Appl. Phys. Lett. 84 (2004) 4298–4300.
[15] S.G. Johnson, J.D. Joannopoulos, Opt. Express 8 (2001) 173–190.
[16] R. Syms, J. Cozens, Optical Guided Waves and Devices, international ed., McGraw-Hill international limited, UK, 1993.
[17] A. Morand, C. Robinson, Y. Desieres, T. Benyattou, P. Benech, O. Jacquin, M. Le Vassor d'Yerville, Opt. Commun. 221 (2003) 353–357.
[18] C.W. Chang, M.L. Wu, W.F. Hsieh, IEEE Photon. Technol. Lett. 15 (2003) 1378–1380.